General Chemical Reaction Network Theory for Olfactory Sensing Based on G-Protein-Coupled Receptors: Elucidation of Odorant Mixture Effects and Agonist-Synergist Threshold

Won Kyu Kim,* Kiri Choi, and Changbong Hyeon Korea Institute for Advanced Study, Hoegiro 85, Dongdaemun-gu, Seoul 02455, Korea

Seogjoo J. Jang[†]

Department of Chemistry and Biochemistry, Queens College,
City University of New York, 65-30 Kissena Boulevard, Queens,
NY 11367 & PhD programs in Chemistry and Physics,
Graduate Center, City University of New York, NY 10016 and
Korea Institute for Advanced Study, Hoegiro 85, Dongdaemun-gu, Seoul 02455, Korea
(Dated: September 6, 2023)

This work presents a general chemical reaction network theory for olfactory sensing processes that employ G-protein-coupled receptors as olfactory receptors (ORs). The theory is applicable to general mixtures of odorants and an arbitrary number of ORs. Reactions of ORs with G-proteins, both in the presence and the absence of odorants, are explicitly considered. A unique feature of the theory is the definition of an odor activity vector consisting of strengths of odorant-induced signals from ORs relative to those due to background G-protein activity in the absence of odorants. It is demonstrated that each component of the odor activity defined this way reduces to a Michaelis–Menten form capable of accounting for cooperation or competition effects between different odorants. The main features of the theory are illustrated for a two-odorant mixture. Known and potential mixture effects, such as suppression, shadowing, inhibition, and synergy are quantitatively described. Effects of relative values of rate constants, basal activity, and G-protein concentration are also demonstrated.

Olfaction, the natural machinery of chemical sensing, [1–6] in general initiates with the activation of a set of olfactory receptors (ORs) by odorants. Activated ORs then generate electrical signals at the neuronal level [2, 3, 7–9], which are further amplified and processed until they are recognized as a sense of smell in the perception space of a brain. Details of how ORs become activated and how signals from ORs are processed may vary between organisms, but the majority of the olfaction consists of a few distinctive information processing stages [4] as shown in Fig. 1. While understanding this level of the mechanism of olfaction is a significant progress that has been achieved through experimental breakthroughs over multiple decades [1–4, 10], many key questions remain unanswered. In particular, there is no well-established and general molecular-level theory capable of explaining the chemical sensitivity, selectivity, and diversity of olfactory sensing [5, 6, 11, 12] yet. Of particular importance is the relationship between odorants-OR

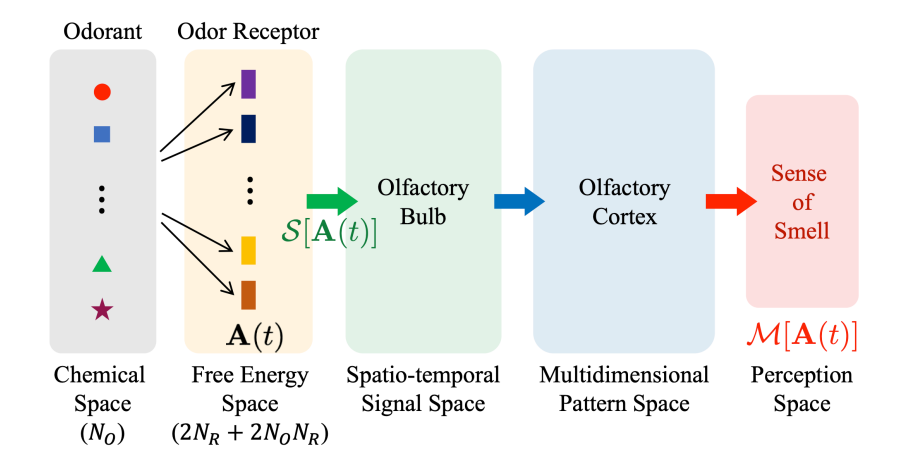


FIG. 1. Schematic of the olfactory process, where a mixture composed of different odorants is introduced to the olfactory system (see the text for details). Odor Receptor means olfactory receptor (OR).

^{*} wonkyukim@kias.re.kr

[†] Seogjoo.Jang@qc.cuny.edu

reactivity and olfactory codes that can also be defined for all distinctive mixtures as well. This letter presents a theory that can serve as such a general framework, upon further refinement and experimental information, by generalizing a recently developed kinetic model of the activation of mammalian ORs [13].

Our previous kinetic model of olfaction[13] was developed for mammals that employ the G-protein-coupled receptors (GPCRs) as ORs and is consistent with known information on GPCRs. [2, 14–21] Important features of this model[13] are as follows. i) The model naturally leads to the Michaelis–Menten type[22] response to the odorant concentrations, which is fully specified by the reaction coefficients and equilibrium constants of underlying reactions that are in principle measurable. ii) All agonistic, antagonistic, and inverse-agonistic behaviors can be described simply by choosing appropriate rate constants. This allows for explaining different ORs with one unifying model. iii) The model suggests that quantifying the EC₅₀ value,[23] which depends on G-protein concentrations, can offer key information of equilibrium constants. Overall, the model can describe essential features of dynamics between a single odorant and OR, based on a standard chemical kinetic theory, while suggesting a prescription for quantitative experimental verification.

The generalization of the kinetic model [13] for multiple odorant–OR pairs, as being developed in this letter, is significant considering recent advances in experimental capability to detect responses to mixtures of odorants [24–28] and relevant theoretical developments [24–26, 28, 29]. In particular, these research outcomes have established that signals generated by ORs due to mixtures of odorants are far from being additive, and cooperative or inhibitory effects between different odorants are fairly common, instead. As a result, even if all the information at the individual odorant-OR level was known, it is not possible to predict the odor codes for the vast majority of mixtures. It is shown that a general kinetic framework of olfactory sensing for multi-component and multi-OR systems can be constructed so as to elucidate the mechanism and extent of the cooperative effect.

We start our formulation from a standard model of the chemical reaction network but with an arbitrary flux of odorant mixtures. We also explicitly express the reactions between ORs and G-proteins, unlike other existing models. Under the assumption of the steady-state limit, which is valid given that there is a clear time scale separation between the flux of odorants and reaction processes involving ORs, we obtain a simple expression for the odor activity from the steady-state concentrations of each odorant, equilibrium constants, and the concentrations of the G-protein. We show that our theory generalizes the theory utilized by Singh *et al.* [26] and consolidates the effects of competition for G-proteins.

The central assumption of our theory is that all the chemical information of odorants retrieved by the olfactory system is entirely encoded into their reactivity with ORs and ensuing changes in the reactivity of ORs with G-proteins. This assumption is well supported by most primary olfactory sensing mechanisms of vertebrates [14, 30]. Under this assumption, the process leading to the downstream signal processing, which starts from the dissociation of G-proteins from ORs, can be modeled by a set of kinetic equations. The scope of our theoretical model is to represent these reactions of ORs, together with odorants and G-proteins, and to establish clear relationships between the overall olfactory sensing activity and reaction parameters.

We here introduce terms representing concentrations and probabilities. We quantify odorants and G-proteins in terms of concentrations, *i.e.*, numbers of molecules per unit volume. On the other hand, we specify ORs of different states in terms of probabilities. This is because the total number of different ORs, denoted as N_R , remains fixed for a given olfactory system. We note that N_R is typically in the range of 100-1000. For example, $N_R \approx 400$ for humans and $N_R \approx 1,000$ for mice [31, 32].

To be more specific, consider an olfactory sensing process where a mixture of different odorants (chemicals) is introduced into the olfactory sensing region (OSR). Let us assume that the mixture consists of N_O different odorants. The concentrations and probabilities of odorants are assumed to be time-dependent for now. Detailed definitions and notations are provided below.

- $C_q(t)$: The concentration of free odorant q within the mixture consisting of N_O odorants, Thus, $q=1,\cdots,N_O$.
- $C_G(t)$: The concentration of free G-proteins.
- $P_n^u(t)$: Probability of the n-th OR in a free state, unbound by any odorant, where $n=1,\cdots,N_R$.
- \bullet $P_n^G(t)$: Probability of the *n*-th OR in a state forming a complex with a G-protein.
- $P_{nq}^c(t)$: Probability of the *n*-th OR in a state bound to an odorant q in its active site. The reactivity of this complex with a G-protein is, in general, significantly different from that of the unbound one.
- $P_{nq}^{cG}(t)$: Probability of the *n*-th OR in a state bound to an odorant q at the active region while also complexed with a G-protein.

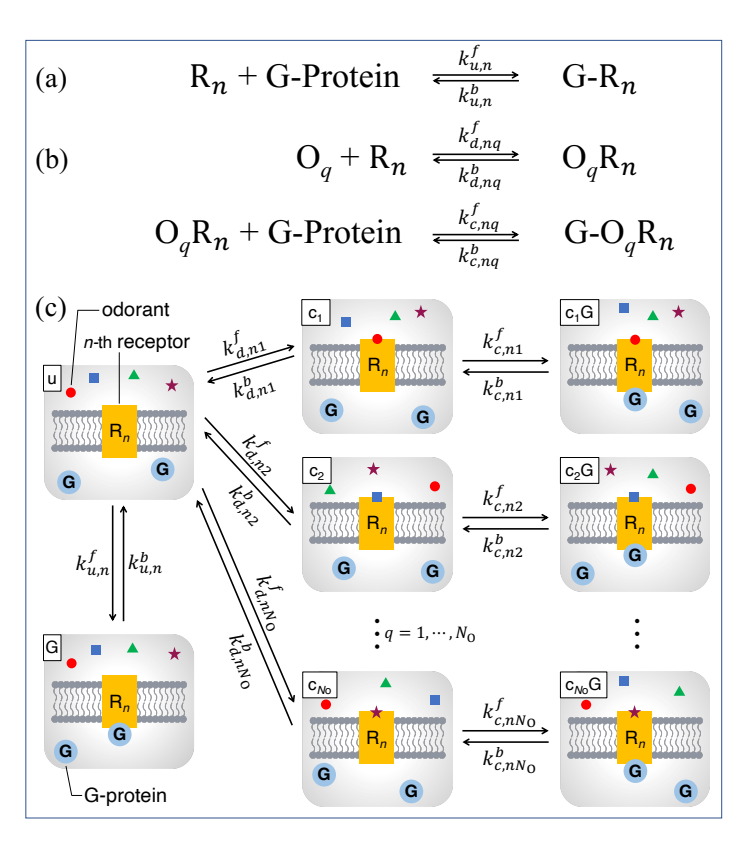


FIG. 2. (a) The reaction of an unbound odor receptor (OR) with a G-protein in the absence of odorants. R_n represents the n-th OR, and $k_{u,n}^f$ and $k_{u,n}^b$ represent coefficients of forward and backward reactions of unbound R_n with a G-protein. (b) Two reactions of an OR in the presence of odorants. Coefficients $k_{d,nq}^f$ and $k_{d,nq}^b$ determine the forward and backward reactions of diffusional encounter of an odorant O_q and the n-th OR, R_n , which controls the production of the unstable complex $O_q R_n$, followed by relaxation of the odorant into the active site. Coefficients $k_{c,nq}^f$ and $k_{c,nq}^b$ control the forward and backward reaction of the complex formation, namely the odorant-OR-G-protein complex G- $O_q R_n$, respectively. (c) Illustration of complete reaction pathways per receptor, given N_O types of odorants.

The sum of all the probabilities for each type of OR has to become unity. Thus, the following constraint for each of $n = 1, \dots, N_R$ has to be satisfied:

$$P_n^u(t) + P_n^G(t) + \sum_{q=1}^{N_O} \left[P_{nq}^c(t) + P_{nq}^{cG}(t) \right] = 1.$$
 (1)

The overall reaction schemes in the presence and absence of odorants are provided in Fig. 2. Detailed rate equations, relevant definitions of rate coefficients, and additional terms are provided below. In this work, we consider idealized chemical reactions and assume that all reaction rate coefficients are independent of time and concentrations.

First, the rate equation governing the concentration of each odorant $q = 1, \dots, N_O$ is given by

$$\frac{dC_{q}(t)}{dt} = I_{q}(t) - \gamma_{q}C_{q}(t)
+ \sum_{n=1}^{N_{R}} \left[k_{d,nq}^{b} P_{nq}^{c}(t) - k_{d,nq}^{f} C_{q}(t) P_{n}^{u}(t) \right],$$
(2)

where $I_q(t)$ is the time-dependent concentration flux (concentration change per unit time) of the q odorant within a mixture introduced into the OSR. The coefficient in the second term, γ_q is the decay rate of the odorant q due to degradation, deactivation, and escape from the OSR. In the second line of the above equation, $k_{d,nq}^f$ is the rate coefficient for the forward rate between the n-th OR and the odorant q leading to the relaxation of the odorant into the active site of the OR, and $k_{d,nq}^b$ is the rate for the backward reaction of the same process.

There are four reactions for each type of OR, involving four different probabilities defined in the last subsection.

First, the rate equation for the probability of free unbound form of the n-th OR is

$$\frac{\mathrm{d}P_n^u(t)}{\mathrm{d}t} = \sum_{q=1}^{N_O} \left[k_{d,nq}^b P_{nq}^c(t) - k_{d,nq}^f C_q(t) P_n^u(t) \right] - k_{u,n}^f C_G(t) P_n^u(t) + k_{u,n}^b P_n^G(t), \tag{3}$$

where the terms in the first line are the same as those in the second line in Eq. (2), namely rate change due to the dissociation from and the association with each odorant. As noted above, this rate represents the combined effect of the diffusional encounter/departure between the odorant and the OR and the relaxation of the former into the active site of the latter. In the second line of the above equation, $k_{u,n}^f$ is the coefficient of the forward reaction rate of the unbound n-th OR forming a complex with a G-protein, and $k_{u,n}^b$ is the coefficient for the backward process, where a G-protein is released from an unbound n-th OR. Note that these two processes are the only reactions that change the probability for the complex between the n-th OR and a G-protein. Thus, for each of $n = 1, \dots, N_R$,

$$\frac{\mathrm{d}P_n^G(t)}{\mathrm{d}t} = k_{u,n}^f C_G(t) P_n^u(t) - k_{u,n}^b P_n^G(t). \tag{4}$$

Similarly, the probability for O_qR_n , the *n*-th OR bound with the odorant q, is governed by the following rate equation:

$$\frac{\mathrm{d}P_{nq}^{c}(t)}{\mathrm{d}t} = k_{d,nq}^{f} C_{q}(t) P_{n}^{u}(t) - k_{d,nq}^{b} P_{nq}^{c}(t)
-k_{c,nq}^{f} C_{G}(t) P_{nq}^{c}(t) + k_{c,nq}^{b} P_{nq}^{cG}(t),$$
(5)

where $k_{d,nq}^f$ and $k_{d,nq}^b$ are defined through Eqs. (2) and (3). In the second line of the above equation, $k_{c,nq}^f$ is the rate coefficient for $O_q R_n$ to be complexed with a G-protein, and $k_{c,nq}^b$ is the rate for the backward process.

The probability for $G-O_qR_n$, the *n*-th OR bound with the odorant q and complexed with a G-protein, is governed by the following rate equation:

$$\frac{\mathrm{d}P_{nq}^{cG}(t)}{\mathrm{d}t} = k_{c,nq}^f C_G(t) P_{nq}^c(t) - k_{c,nq}^b P_{nq}^{cG}(t),\tag{6}$$

where $k_{c,nq}^f$ and $k_{c,nq}^b$ are through Eq. (5).

Lastly, the concentration of the G-protein is governed by the following rate equation:

$$\frac{\mathrm{d}C_{G}(t)}{\mathrm{d}t} = \sum_{n=1}^{N_{R}} \left[-k_{u,n}^{f} C_{G}(t) P_{n}^{u}(t) + k_{u,n}^{b} P_{n}^{G}(t) + \sum_{q=1}^{N_{O}} \left\{ -k_{c,nq}^{f} C_{G}(t) P_{nq}^{c}(t) + k_{c,nq}^{b} P_{nq}^{cG}(t) \right\} \right] + I_{G}(t) - \gamma_{G} C_{G}(t),$$
(7)

where all the rate constants have previously been defined through Eqs. (3)–(5), $I_G(t)$ is the flux of G-proteins provided externally, and γ_G is the decay rate of the G-protein due to degradation and escape from the OSR. We assume that this additional flux and drain mechanisms of G-proteins are much faster than other intermediate rates.

The transduction of the olfactory sensing signal starts from the release of an olfactory signal processing component of the G-protein, known as G_{α} subunit, from G- O_qR_n , the odorant bound OR and G-protein complex. The released G_{α} subunit then initiates a cascade of events [2, 4, 33, 34] that involve cyclic adenosine monophosphate (cAMP) messengers, cyclic nucleotide-gated (CNG) ion channels, and ultimately chloride channels. The depolarization across the membrane of olfactory sensory neurons (OSNs), which primarily involves chloride ions, generates electrical pulses that travel through the OSN and are collected at glomeruli in the olfactory bulb, which are amplified before they are transferred to projection neurons.

It is known that ORs can still bind to G-proteins in the absence of odorants and generate the same signal-processing components of G-proteins, resulting in non-zero background signals (basal activity).[8, 9] Thus, we assume that olfactory signal processing can also result from the dissociation of $G-R_n$, the complex of an OR and a G-protein without odorant, although at a different rate. Therefore, we define the following odor activity from the n-th OR due to interaction with odorant q:

$$a_{nq}(t) = \tau_n \left[k_{c,nq}^b P_{nq}^{cG}(t) + k_{u,n}^b \delta P_n^G(t) \right],$$
 (8)

where τ_n is a multiplicative factor characteristic of the n-th OR and is in the unit of time. The physical meaning of τ_n is that it can be viewed as an "effective time" for the duration of signal processing following G-protein release. Determining this parameter however goes beyond the scope of the chemical network theory presented here. As will become clear below, it is possible to convert the odor activity into a form that does not explicitly need the value of τ_n . $\delta P_n^G(t)$ is the difference between $P_n^G(t)$ in the presence of odorants and the absence of odorants. Then, the odor activity vector for odorant q can be defined as

$$\mathbf{a}_{q}(t) = \begin{pmatrix} a_{1q}(t) \\ \vdots \\ a_{nq}(t) \\ \vdots \\ a_{N_{R}q}(t) \end{pmatrix}. \tag{9}$$

While it is possible to define the individual odor activity for each odorant, what is perceived in the actual olfactory sensing is the sum of all contributions of odorants in a given mixture. Then, we can define the following net odor activity vector for a mixture:

$$\mathbf{A}(t) = \begin{pmatrix} A_1(t) \\ \vdots \\ A_n(t) \\ \vdots \\ A_{N_R}(t) \end{pmatrix}, \tag{10}$$

where

$$A_n(t) = \tau_n \left[\sum_{q=1}^{N_O} k_{c,nq}^b P_{nq}^{cG}(t) + k_{u,n}^b \delta P_n^G(t) \right]. \tag{11}$$

Thus, the odor perception for a mixture of odorants results from the mapping of the net odor activity into the perception space, which we denote as $\mathcal{M}(\mathbf{A}(t))$ (see Fig. 1).

Pending more concrete experimental evidence, it is worth mentioning an important step involved in this mapping process. Due to the allosteric nature of the activation of the CNG ion channels, which can combine up to four cAMPs, and other amplification mechanisms, the actual signal strengths that pass through OSNs for a given mixture of odorants are expected to be different from the odor activity defined above. Since this quantity is experimentally observable, it may be necessary to define the following odor strength for each OR type:

$$S_n(t) = H_n(A_n(t)), \tag{12}$$

where $H_n(x)$ represents an amplification function for each type of OR during neuronal signal generation (see Fig. 1) and is related with the fact that many odor signals can be modeled empirically by Hill function. [24, 25, 29, 43] Possible mechanisms for obtaining such Hill function were provided in our previous work. [43] In addition, considering that the net outcome of odor signal comes from multiple independent actions of numerous ORs, it is also possible that Poisson-type processes can be employed for the modeling of $H_n(x)$ as well. Thus, the detailed form of $H_n(x)$ is expected to be dependent on various details of signal transduction and measurements, and remain an important topic of future theoretical and experimental efforts.

Let us assume that the active olfactory sensing period is preceded by the approach of a steady-state limit, where all the intermediate reactions involving ORs have effectively zero rates on average. Even in the steady-state limit, the odorant concentration C_q is generally time-dependent because Eq. (2) is not zero due to incoming flux $I_q(t)$ and the decay process with rate γ_q . Given that the stationary states of other reaction steps are reached much faster than the time scales of these two processes, the time dependence of $C_q(t_s)$ at the steady-state limit can be determined by

$$C_q(t_s) \approx \int_0^{t_s} d\tau e^{-\gamma_q(t-\tau)} I_q(\tau). \tag{13}$$

A similar relation is assumed for $C_G(t_s)$ as well. Under these assumptions, closed-form expressions for steadystate solutions can be obtained as detailed in Supporting Information (SI). The resulting net odor activity from the interaction between odorant q and the n-th OR is

$$a_{nq} = \frac{\tau_n C_G}{1 + \sum_{q'=1}^{N_O} C_{q'} f_{nq'} + C_G K_{u,n}} \left[C_q k_{c,nq}^f K_{d,nq} - k_{u,n}^f \frac{\sum_{q'=1}^{N_O} C_{q'} f_{nq'}}{1 + C_G K_{u,n}} \right]. \tag{14}$$

TABLE I. Definitions of association constants (ACs) and f_{nq} .

Symbol	Definition
$K_{c,nq} = k_{c,nq}^f / k_{c,nq}^b$	AC for G-protein binding with odorants (Eq. S4 in SI ^a)
$K_{c,nq} = k_{c,nq}^f / k_{c,nq}^b$ $K_{d,nq} = k_{d,nq}^f / k_{d,nq}^b$	AC for odorant binding (Eq. S5 in SI^a)
$K_{u,n} = k_{u,n}^f / k_{u,n}^b$	AC for G-protein binding without odorants (Eq. S13 in SI ^a)
	A function defined in Eq. S9 in SI^a
a Companying Information	

^a Supporting Information.

In the above expression, we used the definitions of the association constants and f_{nq} as shown in Table I. One important feature of Eq. (S24) is that the second term within the square bracket can naturally explain antagonistic and inverse agonistic behaviors.

The set of a_{nq} s expressed as Eq. (S24) completely specifies the odor activity vector \mathbf{a}_q defined by Eq. (9) in the steady-state limit for each pair of odorant and OR. However, what is perceived by the olfactory system is the net odor activity defined by Eq. (10), where each component is given by

$$A_n = \frac{\tau_n C_G}{1 + \sum_{q=1}^{N_O} C_q f_{nq} + C_G K_{u,n}} \left[\sum_{q=1}^{N_O} C_q \left(k_{c,nq}^f K_{d,nq} - \frac{f_{nq} k_{u,n}^f}{1 + C_G K_{u,n}} \right) \right]. \tag{15}$$

This is the main result of our theory for the net activity, and can also be rewritten in the Michaelis-Menten (MM) form:

$$A_n = \frac{\sum_{q=1}^{N_O} a_{nq}^{0,m} C_q / \text{EC}_{50}^{nq}}{1 + \sum_{q=1}^{N_O} C_q / \text{EC}_{50}^{nq}}.$$
(16)

In the above expression, $a_{nq}^{0,m}$ defined by Eq. (S15) in SI is the activity of the *n*-th OR when there is only odorant q in the limit of $C_q \to \infty$. This quantifies the agonistic behavior: $a_{nq}^{0,m} > 0$ for agonistic, $a_{nq}^{0,m} = 0$ for antagonistic, and $a_{nq}^{0,m} < 0$ for inverse-agonistic activities. Importantly, in principle, the net odorant activity can have negative values when the odorant-triggered activity is weaker than the basal activity defined in Eq. (11). Another important quantity EC_{50}^{nq} is the corresponding half-maximum activity concentration of odorant q (see Eq. (S17) in SI). Note that in the MM form, the activity is independent of τ_n because it is rescaled by the maximum activity (see Eq. (S16) in SI).

Equation (16) is similar to the expression suggested by Singh *et al.* [26] However, we have explicitly derived the net activity A_n in the most general manner. In addition, our model can account for the effect of basal activity and incorporates G-protein concentrations into $a_{nq}^{0,m}$ and EC_{50}^{nq} (see SI for more details). Since the derived net activity incorporates inverse-agonistic scenarios, it provides quantitative threshold conditions for various OR responses, which we describe in detail below.

Now, let us consider the case where there are two odorants of types 1 and 2, with corresponding steady-state concentrations C_1 and C_2 . Thus, the total concentration of odorants is $C = C_1 + C_2$, and the mole fraction of odorant 1 is $x_1 = C_1/C$, thereby yielding the mole fraction of odorant 2 as $x_2 = 1 - x_1$.

According to Eq. (16), the net activity in this case is expressed as

$$A_n(C, x_1) = \frac{x_1 \frac{a_{n1}^{0,m}}{EC_{50}^{m1}} + (1 - x_1) \frac{a_{n2}^{0,m}}{EC_{50}^{n2}}}{\frac{1}{C} + \frac{x_1}{EC_{50}^{m1}} + \frac{1 - x_1}{EC_{50}^{n2}}}.$$
(17)

Depending on the agonist condition for each odorant type (determined by the sign and the magnitude of $a_{n1}^{0,m}$ and $a_{n2}^{0,m}$) as well as EC_{50}^{n1} and EC_{50}^{n2} , the odor activity as a function of x_1 changes substantially, and sometimes even qualitatively, as shown in Fig. 3. More comprehensive and detailed calculation results are provided in sections IV and V of SI.

Figure 3(a) illustrates the odor activity when both odorant types are agonistic but type 2 is two-fold stronger $(a_{n1}^{0,m}=5 \text{ and } a_{n2}^{0,m}=10)$. Depending on the ratio $\mathrm{EC}_{50}^{n1}/\mathrm{EC}_{50}^{n2}$, A_n decreases or increases, converging to a value close to $a_{n1}^{0,m}=5$ as x_1 increases to unity. This is because we chose the parameter value $C/\mathrm{EC}_{50}^{n1}=10$, meaning that the odorant concentration is sufficiently large to reach $a_{n1}^{0,m}$ for type 1. Note that the parameter ratio,

$$\frac{\mathrm{EC}_{50}^{n1}}{\mathrm{EC}_{50}^{n2}} = \frac{K_{d,n2}(1 + C_G K_{c,n2})}{K_{d,n1}(1 + C_G K_{c,n1})},\tag{18}$$

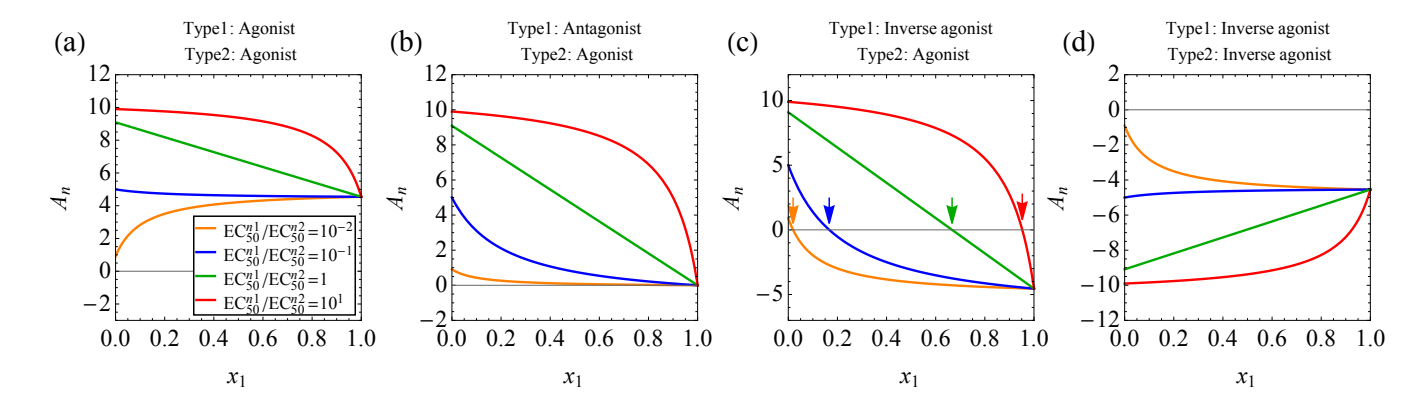


FIG. 3. Odor activity A_n (Eq. (17)) when (a) both types are agonist, (b) type 1: antagonist, type 2: agonist, (c) type 1: inverse agonist, type 2: agonist, and (d) both types are inverse agonist. The arrows in (c) depict the threshold fraction $x_{n1}^{*,ago}$ given in Eq. (19). We use $a_{n1}^{0,m} = 5$ and $a_{n2}^{0,m} = 10$ for the agonist condition, $a_{n1}^{0,m} = a_{n2}^{0,m} = 0$ for the antagonist condition, $a_{n1}^{0,m} = -5$ and $a_{n2}^{0,m} = -10$ for the inverse agonist condition, and $C/EC_{50}^{n1} = 10$. In (a), the red and green curves show "suppression", the blue "overshadowing", and the orange "inhibition". In (b) and (c), all curves show "suppression". In (d), the red and green curves show "suppression", the blue "overshadowing", and the orange "synergy".

is dictated by the odorant binding ratio via $K_{d,n2}/K_{d,n1}$ for small C_G , and approaches $(K_{d,n2}K_{c,n2})/(K_{d,n1}K_{c,n1})$ for large C_G . As $\mathrm{EC}_{50}^{n1}/\mathrm{EC}_{50}^{n2}$ increases, the activity in the limit of vanishing x_1 approaches $a_{n2}^{0,m}=10$, which fulfills the saturation concentration for both types (see the red curve for $\mathrm{EC}_{50}^{n1}/\mathrm{EC}_{50}^{n2}=10$). We observe rich phenomena of activity in Fig. 3(a) depending on different values of $\mathrm{EC}_{50}^{n1}/\mathrm{EC}_{50}^{n2}$: The red and green curves exhibit "suppression," the blue "overshadowing," and the orange "inhibition." Note that the choice of values for $a_{n1}^{0,m}=5$ and $a_{n2}^{0,m}=10$ above, although somewhat arbitrary, are good examples representing the case of two comparable but different odorants, for which rich cooperative and competitive effects are expected. For more comprehensive model calculations including other values of parameters, please refer sections IV and V of SI (see Figs. S2-S4 in SI).

While keeping the identical agonist condition for odorant type 2 ($a_{n2}^{0,m} = 10$), we now consider the antagonist condition ($a_{n1}^{0,m} = 0$) for type 1, as shown in Fig. 3(b). As x_1 increases, the activity indeed decreases to zero, where the decay characteristic is determined by $EC_{50}^{n1}/EC_{50}^{n2}$ and exhibits a "suppression" of activities.

Interestingly, as shown in Fig. 3(c), when the odorant type 1 is inverse agonistic $(a_{n1}^{0,m} = -5)$ and the type 2 is agonistic $(a_{n2}^{0,m} = 10)$, we find a crossover (sign change) of the activity A_n as x_1 changes. This indicates that the agonist condition of the mixture can be tuned (from agonistic to inverse agonistic and vice versa) by changing a fraction of one odorant type. The crossover occurs at the threshold fraction (obtained by solving $A_n = 0$ in Eq. (17)

$$x_{n1}^{*,\text{ago}} = \frac{1}{1 - \frac{a_{n1}^{0,m} EC_{50}^{n2}}{a_{n2}^{0,m} EC_{50}^{n1}}},$$
(19)

which satisfies $0 < x_{n1}^* \le 1$ if and only if $a_{n1}^{0,m}/a_{n2}^{0,m} \le 0$, meaning that the odor activity crossover occurs only in a mixture of agonistic and inverse agonistic odorant types. Although the activity features "suppression" responses for all $\mathrm{EC}_{50}^{n1}/\mathrm{EC}_{50}^{n2}$, the agonistic condition is largely dependent on x_1 [see the arrows in Fig. 3(c)]. We expect this result will be particularly useful for further quantitative studies of odorant-dependent OR response and widespread inhibition. Recently, Inagaki *et al.* have found that the OR response can be largely modulated by changing a fraction of one odorant type in a mixture of agonists and inverse agonists [35]. The OR response can undergo excitatory-to-inhibitory transitions by changing a fraction of inverse agonists in a mixture (see Fig. 4B in Ref. [35]). In addition, Pfister *et al.* have found the inhibitory-to-excitatory transitions of OR response by increasing an agonist fraction in a mixture of agonists and inverse agonists (see Fig. 7B in Ref. [36]). These findings are consistent with A_n in Fig. 3(c) at $\mathrm{EC}_{50}^{n1}/\mathrm{EC}_{50}^{n2} = 10$ (red curve), the threshold of which can be quantitatively determined by Eq. (19). Furthermore, the result enables us to define the following vector for the threshold fraction of odorant type q:

$$\mathbf{x}_{q}^{*,\text{ago}} = \begin{pmatrix} x_{1q}^{*,\text{ago}} \\ \vdots \\ x_{nq}^{*,\text{ago}} \\ \vdots \\ x_{Npq}^{*,\text{ago}} \end{pmatrix}, \tag{20}$$

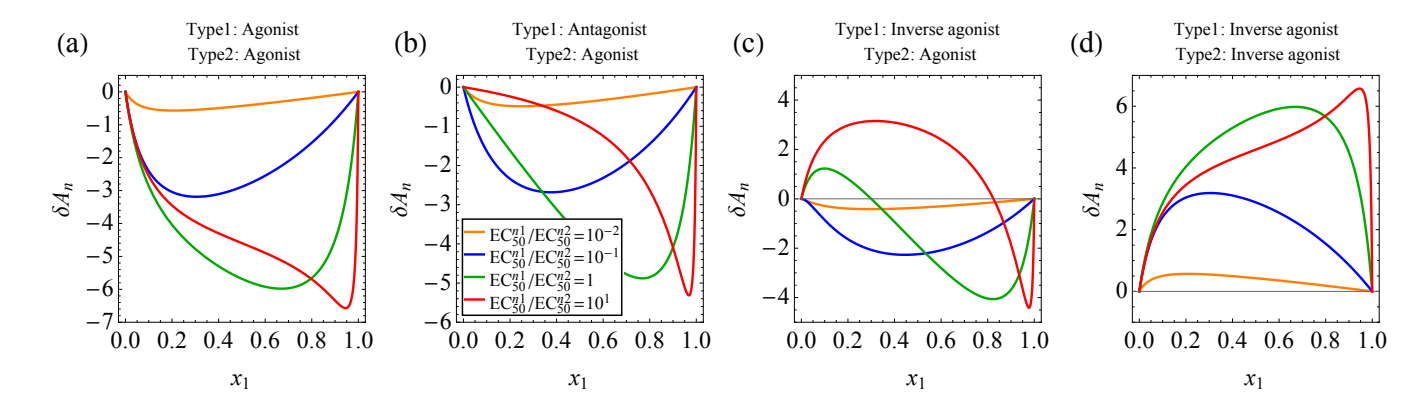


FIG. 4. Relative odor activity δA_n given by Eq. (21) when (a) both types are agonist, (b) type 1: antagonist, type 2: agonist, (c) type 1: inverse agonist, type 2: agonist, and (d) both types are inverse agonist. We use $a_{n1}^{0,m}=5$ and $a_{n2}^{0,m}=10$ for the agonist condition, $a_{n1}^{0,m}=a_{n2}^{0,m}=0$ for the antagonist condition, $a_{n1}^{0,m}=-5$ and $a_{n2}^{0,m}=-10$ for the inverse agonist condition, and $C/\text{EC}_{50}^{n1}=10$.

which provides the transition threshold profile of odor receptors for given odor types in a mixture.

Figure 3(d) shows A_n when both types are inverse agonistic ($a_{n1}^{0,m} = -5$ and $a_{n2}^{0,m} = -10$), which is equal to $-A_n$ of the agonist case shown in Fig. 3(a). We observe that the red and green curves exhibit "suppression", the blue "overshadowing", and the orange "synergy".

Comparing the above net odor activity with those for single-odorant cases can classify different behaviors of a mixture, specifically, the synergistic behavior. Therefore, we define a relative activity

$$\delta A_n(C, x_1) = A_n(C, x_1) - a_{n1}^0(Cx_1) - a_{n2}^0[C(1 - x_1)],$$

where $a_{n1}^0(Cx_1)$ is the odor activity for odorant 1 at concentration Cx_1 in the absence of odorant 2, and $a_{n2}^0[C(1-x_1)]$ is the odor activity for odorant 2 at concentration $C(1-x_1)$ in the absence of odorant 1. Then, we find

$$\delta A_n(C, x_1) = \frac{-C^2 \frac{x_1(1-x_1)}{\text{EC}_{50}^{n_1} \text{EC}_{50}^{n_2}}}{1 + C\left(\frac{x_1}{\text{EC}_{50}^{n_1}} + \frac{1-x_1}{\text{EC}_{50}^{n_2}}\right)} \left(\frac{a_{n1}^{0,m}}{1 + C\frac{x_1}{\text{EC}_{50}^{n_1}}} + \frac{a_{n2}^{0,m}}{1 + C\frac{1-x_1}{\text{EC}_{50}^{n_2}}}\right). \tag{21}$$

Figure 4(a) depicts δA_n when both odorant types are agonistic $(a_{n1}^{0,m}=5 \text{ and } a_{n2}^{0,m}=10)$, which is the same condition as given in Fig. 3(a). We find that δA_n is always negative. Thus, the net odor activity is always smaller than the direct algebraic sum of independent and individual activities. This suggests that a synergistic enhancement is impossible (anti-synergistic).

When the odorant type 1 is antagonistic and type 2 is agonistic $(a_{n1}^{0,m}=0 \text{ and } a_{n2}^{0,m}=10)$, we find a similar anti-synergistic condition [see Fig. 4(b)]. However, when odorant type 1 is inverse agonistic $(a_{n1}^{0,m}=-5)$ and type 2 is agonistic $(a_{n2}^{0,m}=10)$, we find a large variation of δA_n [Fig. 4(c)]. Depending on x_1 and $\mathrm{EC}_{50}^{n1}/\mathrm{EC}_{50}^{n2}$, the net activity can be synergistic $(\delta A_n>0)$ or anti-synergistic $(\delta A_n<0)$. The threshold synergistic condition is found as

$$x_{n1}^{*,\text{syn}} = \frac{1 + \frac{a_{n_1}^{0,m} \text{EC}_{50}^{22}}{a_{n_1}^{0,m} C} + \frac{\text{EC}_{50}^{n_2}}{C}}{1 - \frac{a_{n_1}^{0,m} \text{EC}_{50}^{n_2}}{a_{n_1}^{0,m} \text{EC}_{50}^{n_2}}},$$
(22)

which satisfies $0 < x_{n1}^{*,\mathrm{syn}} \le 1$ if and only if $a_{n1}^{0,m}/a_{n2}^{0,m} \le 0$. The odor activation is synergistic in the range of $0 < x_1 < x_{n1}^{*,\mathrm{syn}}$, where the range becomes larger as $\mathrm{EC}_{50}^{n1}/\mathrm{EC}_{50}^{n2}$ increases and vice versa for the anti-synergistic range. The change of $\delta A_n(x_1)$ is substantial, particularly resulting in qualitative difference for large $\mathrm{EC}_{50}^{n1}/\mathrm{EC}_{50}^{n2}$, where the slope of the decaying curve at the crossover point becomes sharper. This implies that a small change in x_1 can significantly modulate the synergistic condition.

In Fig. 4(d), when both types are inverse agonistic $(a_{n1}^{0,m} = -5 \text{ and } a_{n2}^{0,m} = -10)$, $\delta A_n(x_1)$ is identical to $-\delta A_n$ in the agonist case shown in Fig. 4(a). Note that in our model the synergistic activity occurs only when the mixture contains an inverse agonist. This means that the synergistic effect in a GPCR-based signal downstream is dictated

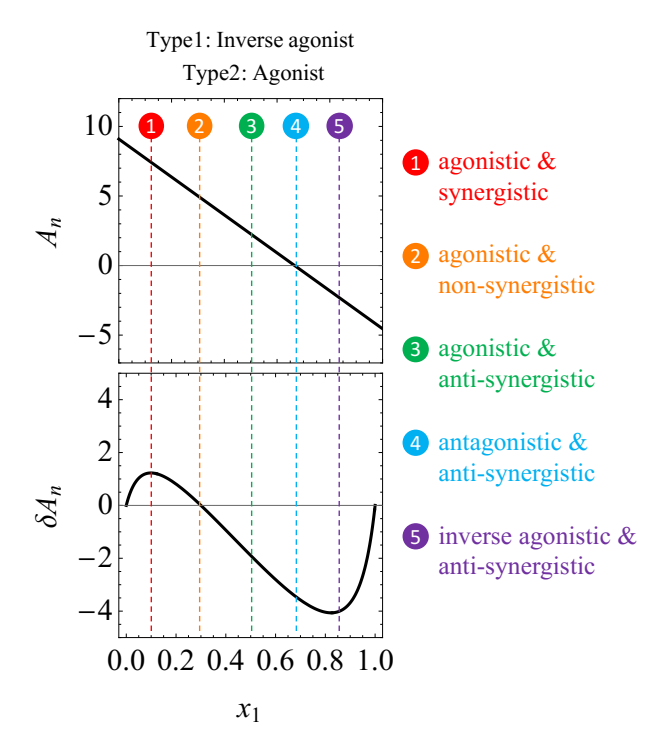


FIG. 5. Agonist–synergist condition for a mixture of inverse agonists (type 1: $a_{n1}^{0,m} = -5$) and agonists (type 2: $a_{n2}^{0,m} = 10$) at $EC_{50}^{n1}/EC_{50}^{n2} = 1$ and $C/EC_{50}^{n1} = 10$, which depends on x_1 . Five different scenarios are depicted by numeric indices. 1: Agonistic and synergistic, 2: Agonistic and non-synergistic, 3: Agonistic and anti-synergistic, 4: Antagonistic and anti-synergistic, and 5: Inverse agonistic and anti-synergistic.

by the number of inhibitory encounters (odorants, ligands, or drugs). Moreover, the synergistic threshold vector,

$$\mathbf{x}_{q}^{*,\text{syn}} = \begin{pmatrix} x_{1q}^{*,\text{syn}} \\ \vdots \\ x_{nq}^{*,\text{syn}} \\ \vdots \\ x_{N_{R}q}^{*,\text{syn}} \end{pmatrix}, \tag{23}$$

provides a synergistic threshold profile of odor receptors given the odor types in a mixture. This result offers insights into a quantitative understanding of OR-dependent response and synergy criteria. Recently, Inagaki *et al.* have found that depending on ORs, the odor activity response by an identical mixture can be considerably different—"suppression" or "synergy" (see Fig. 6B in Ref. [35]). What is notable is that the synergistic activity has been found from the OR response by a mixture of agonists and inverse agonists in the experiment, which is consistent with our theoretical model (*e.g.*, see scenario 1 in Fig. 5).

It is worthwhile to explain several important points relevant to our main results. For mammalian olfactory GPCR signaling, the concentration of G-proteins in an OSN is known to be ~ 1 mM [37, 38]. In addition, a success probability of odorant-triggered signal downstream from GPCR to G-protein is found to be very low ($\sim 10^{-4}$) [37]. This suggests that the ratio $\mathrm{EC}_{50}^{n1}/\mathrm{EC}_{50}^{n2}$ given in Eq. (18) for olfactory sensing becomes

$$\frac{\mathrm{EC}_{50}^{n1}}{\mathrm{EC}_{50}^{n2}} = \frac{K_{d,n2}}{K_{d,n1}},\tag{24}$$

where the key factor determining the agonist-synergist condition is the odorant-binding (association) constant.

Figure 5 shows the agonist–synergist condition depending on the mole fraction x_1 of odorant type 1 based on the net activity A_n and the relative activity δA_n for a mixture of inverse agonists (type 1: $a_{n1}^{0,m}=-5$) and agonists (type 2: $a_{n2}^{0,m}=10$) at $\mathrm{EC}_{50}^{n1}/\mathrm{EC}_{50}^{n2}=1$ and $C/\mathrm{EC}_{50}^{n1}=10$. Various scenarios are possible: 1: Agonistic and synergistic, 2: Agonistic and non-synergistic, 3: Agonistic and anti-synergistic, 4: Antagonistic and anti-synergistic, and 5: Inverse agonistic and anti-synergistic conditions. In general, these conditions are determined by the threshold space

 $(\mathbf{x}_q^{*,\mathrm{ago}},\mathbf{x}_q^{*,\mathrm{syn}})$ given by Eqs. (19) and (23), which can be measured in experiments in terms of the Michaelis–Menten parameters.

Interestingly, agonist–synergist modulation becomes significant when there are inhibitory ligands, i.e., inverse-agonistic odorants, in the mixture. A noteworthy crossover between the net and the relative activities occurs only when a pair of agonists and inverse agonists compose the two-odorant mixture. We found the agonist–synergist condition can be tuned by changing a mole fraction of one odorant in a mixture. This is in line with previous observations of "competitive antagonism" and "widespread modulation", [39, 40] where antagonists or inverse agonists [41] in the odorant mixture modulate the signal downstream.

Various theoretical models [24, 29, 39, 40, 42, 43], mostly based on the Hill equation as an empirical formula, have been used to understand the odorant-dependent modulation of receptor reaction by mixtures. Recently, Singh *et al.* presented the "competitive-binding" model [26] based on the Michaelis–Menten equation similar to what we derived previously [13] and is extended here, and showed possible widespread modulation of ORs in an equimolar mixture $(x_1=x_2=1/2)$. Our model provides further information on microscopic parameters, such as G-protein concentrations, association constants, and more importantly, the basal activity, and can serve as a general framework for understanding the model by Singh *et al.* [26]

It should be noted that experimental observations point towards a broad range of basal activities across different types of OSNs [35, 44, 45]. We find that $C_GK_{u,n}$ is crucial for determining the basal activity. For low basal activity, the probability for G-proteins to bind to an OR in the absence of odorants (Eq. (S22) in SI) is small, which vanishes as $C_GK_{u,n} \to 0$. Instead, for large $C_GK_{u,n}$, the basal activity is high. Therefore, EC_{50}^{nq} (Eq. (S17) in SI) turns out to depend on the basal activity, while the ratio $\mathrm{EC}_{50}^{n1}/\mathrm{EC}_{50}^{n2}$ for a mixture is independent of the basal activity. This finding may be useful for quantitative analyses of olfactory sensing with mixtures.

In conclusion, in this work, we generalized the rate equations for multi-odorant and multi-OR reactions by explicitly incorporating the effects of odorant binding, G-protein binding, and basal activity. The resultant analytical solutions yield the net activity and relative activity expressed in terms of the Michaelis-Menten equation, with corresponding microscopic biochemical contributions as functions of x_1 and C_G . Our theory provides mechanisms and quantitative criteria for the important effects of odorant mixtures. In addition, our main theoretical results can be used to construct feature space of odorants based on their reactivity with ORs. Thus, our theory, along with recent experimental progress to objectively measure odor codes at the neuronal level, [6] can be utilized for the development of more efficient and experimentally verifiable Machine Learning approaches for olfaction since the space of chemical rates and equilibrium constants can serve as an effective feature space for modeling olfactory codes.

While our theory describes the effects of competitive multi-odorant binding and G-protein binding for olfactory GPCR signaling, the underlying model can also be adapted to provide a general framework for elucidating similar GPCR-based ligand-receptor-effector reaction processes with ligand mixtures, e.g., gustatory sensing [46] and behavioral regulation with a mixture of neurotransmitters [47]. It is important to note that our assumption that combines a diffusional encounter of odorant and OR, as well as the relaxation of the former into an active site of the latter as a single-step process, might be drastic simplification. Nonetheless, considering that this process is likely to be faster than the diffusional encounter and the reaction of the unbound OR with a G-protein, it is reasonable to represent the two processes by a single rate equation. Even in the case where these assumptions do not hold, it is still possible to explicitly represent the two processes into two separate rate equations, which introduces an additional equilibrium constant in the steady-state limit. We expect that further refinement of our model with an increasing number of experimental data is possible. The present results are based on the steady-state solutions, which are important but yet describe only a fraction of our kinetic model. For longer time scales, one can incorporate the dynamics of concentrations of odorants and G-proteins, as given by Eqs. (2) and (7), which will provide a more comprehensive perspective to understand the kinetics of olfactory sensing throughout a wide temporal range.

ACKNOWLEDGEMENT

SJJ acknowledges major support from the National Science Foundation (CHE-1900170) and Korea Institute for Advanced Study (KIAS) for partial support through KIAS scholar program. Additional support came from KIAS Individual Grants CG076002 (WKK), CG077002 (KC), and CG035003 (CH). We thank the Center for Advanced Computation in KIAS for providing the computing resources.

^[1] M. Zarzo, The sense of smell: molecular basis of odorant recognition, Biol. Rev. 82, 455 (2007).

^[2] S. DeMaria and J. Ngai, The cell biology of smell, J. Cell Biol. 191, 443 (2010).

- [3] K. Mori and H. Sakano, How is the olfactory map formed and interpreted in the mammalian brain?, Annu. Rev. Neurosci. **34**, 467 (2011).
- [4] A. Tromelin, Odour perception: A review of an intricate signalling pathway, Flavour Fragr. J. 31, 107 (2016).
- [5] E. Block, Molecular basis of mammalian odor discrimination: A status report, J. Agric. Food Chem. 66, 13346 (2018).
- [6] L. Xu, D.-J. Zou, and S. Firestein, Odor mixtures: A chord with silent notes, Front. Ecol. Evol. 11, 1135486 (2023).
- [7] V. Bhandawat, J. Reisert, and K.-W. Yau, Elementary response of olfactory receptor neurons to odorants, Science 308, 1931 (2005).
- [8] V. Bhandawat, J. Reisert, and K.-W. Yau, Signaling by olfactory receptor neurons near threshold, Proc. Natl. Acad. Sci. U.S.A. 107, 18682 (2010).
- [9] Y. Ben-Chaim, M. M. Cheng, and K.-W. Yau, Unitary response of mouse olfactory receptor neurons, Proc. Natl. Acad. Sci. U.S.A. 108, 822 (2011).
- [10] L. Buck and R. Axel, A novel multigene family may encode odorant receptors: a molecular basis for odor recognition, Cell **65**, 175 (1991).
- [11] Y. Li, Z. Peterlin, J. Ho, T. Yarnitzky, M. T. Liu, M. Fichman, M. Y. Niv, H. Matsunami, S. Firestein, and K. Ryan, Aldehyde recognition and discrimination by mammalian odorant receptors via functional group-specific hydration chemistry, ACS Chem. Biol. 9, 2563 (2014).
- [12] S. A. Stanislav A. Pshenichnyuk, R. G. Rakhmeyev, N. L. Asfandiarov, A. S. Komolov, A. Modelli, and D. Jones, Can the electron-accepting properties of odorants be involved in their recognition by the olfactory system?, J. Phys. Chem. Lett. 9, 2320 (2018).
- [13] S. Jang and C. Hyeon, Kinetic model for the activation of mammalian olfactory receptor, J. Phys. Chem. B 121, 1304 (2017).
- [14] C. Bushdid, C. A. de March, S. Fiorucci, H. Matsunami, and J. Golebiowski, Agonists of g-protein-coupled odorant receptors are predicted from chemical features, J. Phys. Chem. Lett. 9, 2235 (2018).
- [15] C. A. de March, S.-K. Kim, S. Antonczak, W. A. Goddard III, and J. Golebiowski, G protein-coupled odorant receptors: From sequence to structure, Protein Sci. 24, 1543 (2015).
- [16] W. Huang, A. Manglik, A. Venkatakrishnan, T. Laeremans, E. N. Feinberg, A. L. Sanborn, H. E. Kato, K. E. Livingston, T. S. Thorsen, R. C. Kling, et al., Structural insights into μ-opioid receptor activation, Nature 524, 315 (2015).
- [17] R. Sounier, C. Mas, J. Steyaert, T. Laeremans, A. Manglik, W. Huang, B. K. Kobilka, H. Déméné, and S. Granier, Propagation of conformational changes during μ-opioid receptor activation, Nature 524, 375 (2015).
- [18] A. Manglik, T. H. Kim, M. Masureel, C. Altenbach, Z. Yang, D. Hilger, M. T. Lerch, T. S. Kobilka, F. S. Thian, W. L. Hubbell, et al., Structural insights into the dynamic process of β2-adrenergic receptor signaling, Cell 161, 1101 (2015).
- [19] R. O. Dror, A. C. Pan, D. H. Arlow, D. W. Borhani, P. Maragakis, Y. Shan, H. Xu, and D. E. Shaw, Pathway and mechanism of drug binding to g-protein-coupled receptors, Proc. Natl. Acad. Sci., U.S.A. 108, 13118 (2011).
- [20] Y. Lee, S. Kim, S. Choi, and C. Hyeon, Ultraslow water-mediated transmembrane interactions regulate the activation of a2a adenosine receptor, Biophys. J. 111, 1180 (2016).
- [21] Y. Lee, S. Choi, and C. Hyeon, Communication over the network of binary switches regulates the activation of a2a adenosine receptor, PLOS Comp. Biol. 11, e1004044 (2015).
- [22] Cornish-Bowden, One hundred years of michaelis-menten kinetics, Perspect. Sci. 4, 3 (2015).
- [23] Defined as the concentration of the odorant where the signal strength becomes half the maximum.
- [24] G. Cruz and G. Lowe, Neural coding of binary mixtures in a structurally related odorant pair, Sci. Rep. 3, 1220 (2013).
- [25] G. Reddy, J. D. Zak, M. Vergassola, and V. N. Murthy, Antagonism in olfactory receptor neurons and its implications for the perception of odor mixtures, eLife 7, e34958 (2018).
- [26] V. Singh, N. R. Murphy, V. Balasubramanian, and J. D. Mainland, Competitive binding predicts nonlinear responses of olfactory receptors to complex mixtures, Proc. Natl. Acad. Sci., U.S.A. 116, 9598 (2019).
- [27] L. Xu, W. Li, V. Voleti, D.-J. Zou, E. M. Hillman, and S. Firestein, Widespread receptor-driven modulation in peripheral olfactory coding, Science 368, eaaz5390 (2020).
- [28] S. M. Kurian, R. G. Naressi, D. Manoel, A.-S. Barwich, B. Malnic, and L. R. Saraiva, Odor coding in the mammalian olfactory epithelium, Cell Tissue Res. **383**, 445 (2021).
- [29] A. Marasco, A. De Paris, and M. Migliore, Predicting the response of olfactory sensory neurons to odor mixtures from single odor response, Sci. Rep. 6, 24091 (2016).
- [30] M. Spehr and S. D. Munger, Olfactory receptors: G protein-coupled receptors and beyond, J. Neurochem. 109, 1570 (2009).
- [31] Y. Niimura and M. Nei, Evolutionary dynamics of olfactory and other chemosensory receptor genes in vertebrates, J. Hum. Genet. 51, 505 (2006).
- [32] C. B. Billesbølle, C. A. de March, W. J. van der Velden, N. Ma, J. Tewari, C. L. Del Torrent, L. Li, B. Faust, N. Vaidehi, H. Matsunami, et al., Structural basis of odorant recognition by a human odorant receptor, Nature 615, 742 (2023).
- [33] D. M. Rosenbaum, S. G. Rasmussen, and B. K. Kobilka, The structure and function of g-protein-coupled receptors, Nature 459, 356 (2009).
- [34] N. F. Berbari, A. K. O'Connor, C. J. Haycraft, and B. K. Yoder, The primary cilium as a complex signaling center, Curr. Biol. 19, R526 (2009).
- [35] S. Inagaki, R. Iwata, M. Iwamoto, and T. Imai, Widespread inhibition, antagonism, and synergy in mouse olfactory sensory neurons in vivo, Cell Rep. 31 (2020).
- [36] P. Pfister, B. C. Smith, B. J. Evans, J. H. Brann, C. Trimmer, M. Sheikh, R. Arroyave, G. Reddy, H.-Y. Jeong, D. A. Raps, et al., Odorant receptor inhibition is fundamental to odor encoding, Curr. Biol. 30, 2574 (2020).

- [37] R.-C. Li, L. L. Molday, C.-C. Lin, X. Ren, A. Fleischmann, R. S. Molday, and K.-W. Yau, Low signaling efficiency from receptor to effector in olfactory transduction: A quantified ligand-triggered gpcr pathway, Proc. Natl. Aca. Sci., U.S.A. **119**, e2121225119 (2022).
- [38] R. W. Rodieck, The first steps in seeing. (Sinauer Associates, 1998).
- [39] G. Reddy, J. D. Zak, M. Vergassola, and V. N. Murthy, Antagonism in olfactory receptor neurons and its implications for the perception of odor mixtures, eLife 7, e34958 (2018).
- [40] L. Xu, D.-J. Zou, and S. Firestein, Odor mixtures: A chord with silent notes, Front. Ecol. Evol. 11, 1135486 (2023).
- [41] C. A. de March, W. B. Titlow, T. Sengoku, P. Breheny, H. Matsunami, and T. S. McClintock, Modulation of the combinatorial code of odorant receptor response patterns in odorant mixtures, Mol. Cell. Neurosci. 104, 103469 (2020).
- [42] J.-P. Rospars, P. Lansky, M. Chaput, and P. Duchamp-Viret, Competitive and noncompetitive odorant interactions in the early neural coding of odorant mixtures, J. Neurosci. 28, 2659 (2008).
- [43] J. H. Bak, S. J. Jang, and C. Hyeon, Implications for human odor sensing revealed from the statistics of odorant-receptor interactions, PLOS Comput. Biol. 14, e1006175 (2018).
- [44] J. Reisert, Origin of basal activity in mammalian olfactory receptor neurons, J. Gen. Physiol. 136, 529 (2010).
- [45] M. Mistry, E. Theodorou, S. Schaal, and M. Kawato, Optimal control of reaching includes kinematic constraints, J. Neurophysiol. 110, 1 (2013).
- [46] S. K. McLaughlin, P. J. McKinnon, and R. F. Margolskee, Gustducin is a taste-cell-specific g protein closely related to the transducins, Nature **357**, 563 (1992)
- [47] J. D. McCorvy and B. L. Roth, Structure and function of serotonin g protein-coupled receptors, Pharmacol. Ther. 150, 129 (2015).

SUPPORTING INFOMATION

Solution of rate equations in the steady-state limit

We consider the steady-state limit where all the rate equations involving the intermediates in the main text become zero. Although the concentrations can still be time-dependent, for notational convenience, we drop all the concentrations with such time dependence.

Let us first start from the conditions that Eqs. 5 and 6 become zero. From the condition that Eq. 6 is zero, we obtain

$$k_{c,nq}^f P_{nq}^c C_G = k_{c,nq}^b P_{nq}^{cG}.$$
 (S1)

Combining the above condition with the condition that Eq. 5 is zero and rearranging terms, we find that

$$P_{nq}^{c} = \frac{k_{d,nq}^{f}}{k_{d,nq}^{b}} C_{q} P_{n}^{u}. \tag{S2}$$

Employing the above expression in Eq. S1, we find that

$$P_{nq}^{cG} = \frac{k_{c,nq}^f}{k_{c,nq}^b} \frac{k_{d,nq}^f}{k_{d,nq}^b} C_q C_G P_n^u.$$
 (S3)

Now let us define the following equilibrium constants

$$K_{c,nq} = \frac{k_{c,nq}^f}{k_{c,nq}^b},\tag{S4}$$

$$K_{d,nq} = \frac{k_{d,nq}^f}{k_{d,nq}^b}.$$
 (S5)

With the above definitions, Eqs. S2 and S3 can be expressed as

$$P_{nq}^c = K_{d,nq} C_q P_n^u, (S6)$$

$$P_{nq}^{c} = K_{d,nq} C_{q} P_{n}^{u},$$

$$P_{nq}^{cG} = K_{d,nq} K_{c,nq} C_{q} C_{G} P_{n}^{u}.$$
(S6)

Combining Eqs. S6 and S7, we obtain

$$P_{nq}^c + P_{nq}^{cG} = C_q f_{nq} P_n^u, (S8)$$

where

$$f_{nq} = K_{d,nq} \left[1 + C_G K_{c,nq} \right].$$
 (S9)

Note that f_{nq} defined by Eq. S9 is a linear function of the concentration of G-protein, C_G , which is determined by the specific physiological condition in the olfactory regions. All other parameters in f_{nq} are fully determined by equilibrium coefficients.

Employing Eq. S8 in the normalization condition, Eq. 1, we obtain

$$P_n^u = \frac{1 - P_n^G}{1 + \sum_{q=1}^{N_O} C_q f_{nq}}.$$
 (S10)

The above equation provides a relationship between P_n^u and P_n^G , probabilities of completely unbound OR and G-protein-only bound OR in the steady-state limit. Combining this information with the condition that Eq. 4 is also zero in the steady-state limit, we obtain the following expression

$$P_n^G = \frac{C_G K_{u,n}}{1 + \sum_{q=1}^{N_O} C_q f_{nq} + C_G K_{u,n}},$$
(S11)

$$P_n^u = \frac{1}{1 + \sum_{q=1}^{N_O} C_q f_{nq} + C_G K_{u,n}},$$
 (S12)

where

$$K_{u,n} = \frac{k_{u,n}^f}{k_{u,n}^b}. (S13)$$

B. Single odorant case

We here consider the case where $N_O = 1$ with only odorant q, for which Eq. S24 reduces to

$$a_{nq}^{0} = \frac{\tau_{n}C_{G}C_{q}}{1 + C_{q}f_{nq} + C_{G}K_{u,n}} \times \left[k_{c,nq}^{f}K_{d,nq} - \frac{f_{n,q}k_{u,n}^{f}}{1 + C_{G}K_{u,n}}\right].$$
(S14)

In the limit where $C_q \to \infty$, the above quantity reaches the following maximum:

$$a_{nq}^{0,m} = \frac{\tau_n C_G}{f_{nq}} \left[k_{c,nq}^f K_{d,nq} - \frac{f_{nq} k_{u,n}^f}{1 + C_G K_{u,n}} \right]. \tag{S15}$$

Therefore,

$$\frac{a_{nq}^{0}}{a_{nq}^{0,m}} = \frac{C_{q}f_{nq}}{1 + C_{q}f_{nq} + C_{G}K_{u,n}}$$

$$\equiv \frac{C_{q}}{EC_{50}^{nq} + C_{q}}, \tag{S16}$$

where EC_{50}^{nq} is the concentration of odorant q for which its odor activity with the n-th OR becomes half of its maximum and is expressed as

$$EC_{50}^{nq} = \frac{1 + C_G K_{u,n}}{f_{nq}}$$

$$= \frac{1 + C_G K_{u,n}}{K_{d,nq} (1 + C_G K_{c,nq})}.$$
(S17)

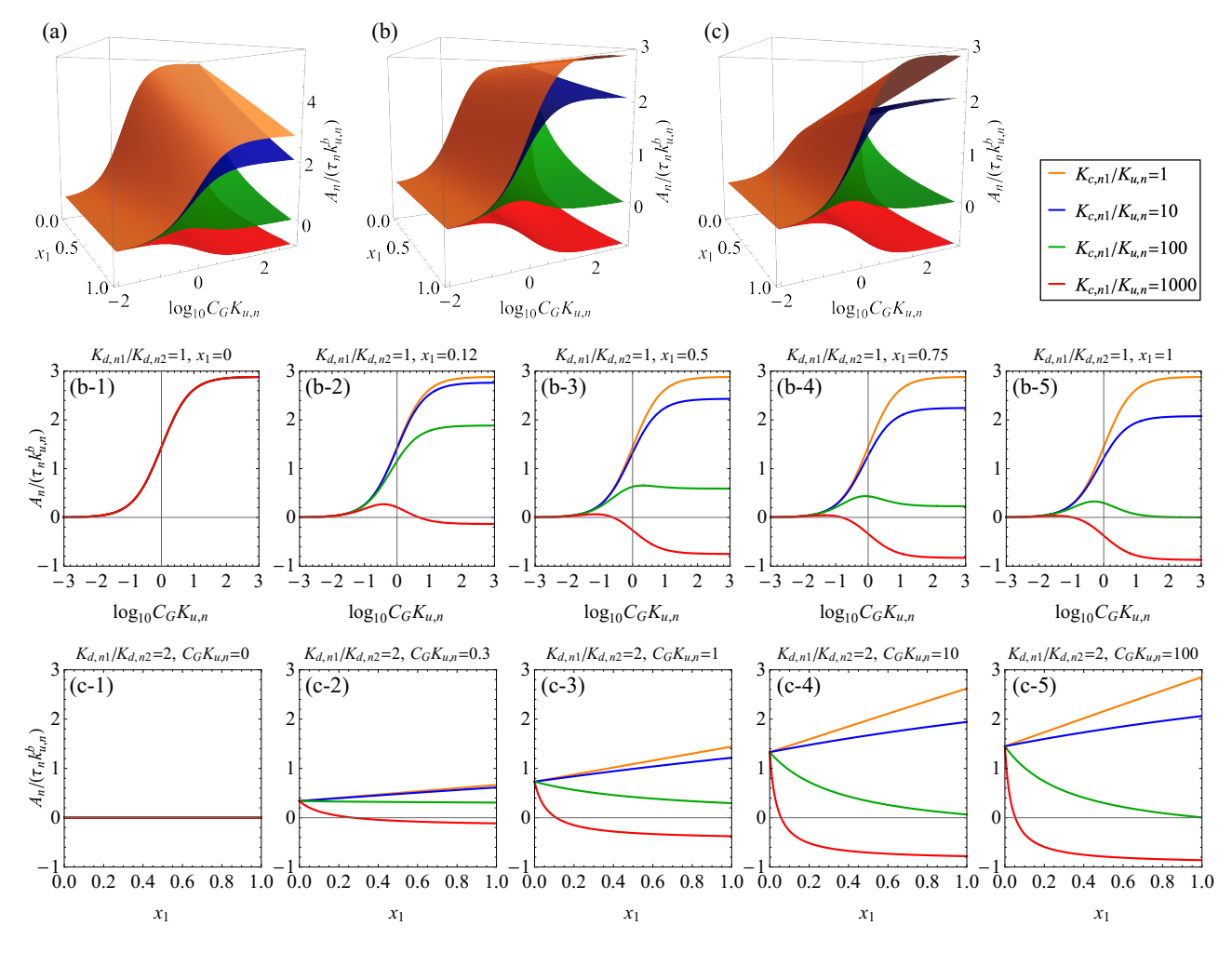


FIG. S1. Odor activity $\tilde{A}_n(\tilde{C}_G, x_1)$ in Eq. S25 at (a) $K_{d,n1}/K_{d,n2}=0.5$, (b) $K_{d,n1}/K_{d,n2}=1$, and (c) $K_{d,n1}/K_{d,n2}=2$ for different values of $K_{c,n1}/K_{u,n}$. Middle row: Odor activity $\tilde{A}_n(\tilde{C}_G)$ at $K_{d,n1}/K_{d,n2}=1$ [panel (b)] for (b-1) $x_1=0$, (b-2) $x_1=0.12$, (b-3) $x_1=0.5$, (b-4) $x_1=0.75$, and (b-5) $x_1=1$. Bottom row: Odor activity $\tilde{A}_n(x_1)$ at $K_{d,n1}/K_{d,n2}=2$ [panel (c)] for (c-1) $\tilde{C}_G=0$, (c-2) $\tilde{C}_G=0.1$, (c-3) $\tilde{C}_G=1$, (c-4) $\tilde{C}_G=10$, and (c-5) $\tilde{C}_G=100$. We use $k_{c,n1}^f/k_{u,n}^f=k_{c,n2}^f/k_{u,n}^f=100$, $K_{c,n2}/K_{u,n}=1$, and $CK_{d,n1}=0.03$.

Employing Eq. S17, we can express f_{nq} in terms of EC_{50}^{nq} as follows:

$$f_{nq} = \frac{1 + C_G K_{u,n}}{EC_{50}^{nq}}. ag{S18}$$

Using this expression in Eq. S15 and rearranging terms, we find the following expression:

$$\tau_n C_G k_{c,nq}^f K_{d,nq} = \frac{a_{nq}^{0,m} (1 + C_G K_{u,n})}{E C_{50}^{nq} - K_{nq}},$$
(S19)

where

$$K_{nq} = \frac{k_{u,n}^f}{k_{c,nq}^f K_{d,nq}}.$$
 (S20)

C. Derivation of a_n and A_n

Under the steady-state condition with Eq. 13, simple expressions for steady-state solutions can be obtained as detailed in Supporting Information. The resulting solutions for probabilities, dropping the explicit dependences on t_s for notational convenience, are given by Eqs. S11 and S12. Equation S12 can be combined with Eq. S7 to determine the steady-state value of P_{nq}^{cG} that is needed for the calculation of the first term in the odor activity defined by Eq. 8. Thus, we obtain the following expression:

$$P_{nq}^{cG} = \frac{K_{d,nq} K_{c,nq} C_q C_G}{1 + \sum_{q=1}^{N_O} C_q f_{nq} + C_G K_{u,n}},$$
 (S21)

where $K_{c,nq}$, $K_{d,nq}$, f_{nq} , and $K_{u,n}$ are defined by Eqs. S4, S5, S9, and S13, respectively.

For the calculation of the second term in Eq. 8, we also need to determine the steady-state value of P_n^G in the absence of odorants. This can be obtained by setting $C_q = 0$ for all q in Eq. S11, which results in the following expression:

$$P_{n,0}^G = \frac{C_G K_{u,n}}{1 + C_G K_{u,n}}. (S22)$$

Subtracting this from Eq. S11, we obtain

$$\delta P_n^G = -\frac{\left(\sum_{q=1}^{N_O} C_q f_{nq}\right) C_G K_{u,n}}{\left(1 + \sum_{q=1}^{N_O} C_q f_{nq} + C_G K_{u,n}\right) \left(1 + C_G K_{u,n}\right)}.$$
(S23)

Using Eqs. S21 and S23 in Eq. 8 result in the following steady-state expression for the odor activity from the interaction between odorant q and the n-th OR:

$$a_{nq} = \frac{\tau_n C_G}{1 + \sum_{q'=1}^{N_O} C_{q'} f_{nq'} + C_G K_{u,n}} \times \left[C_q k_{c,nq}^f K_{d,nq} - k_{u,n}^f \frac{\sum_{q'=1}^{N_O} C_{q'} f_{nq'}}{1 + C_G K_{u,n}} \right].$$
 (S24)

D. Net odor activity depending on C_G and x_1

For a two-odorant mixture, the net odor activity A_n in Eq. 15 is rewritten in a dimensionless form:

$$\tilde{A}_{n} = \frac{x_{1}\tilde{K}_{d,n1}\left(\tilde{k}_{c,n1}^{f} - \Gamma_{1}\right) + (1 - x_{1})\tilde{K}_{d,n2}\left(\tilde{k}_{c,n2}^{f} - \Gamma_{2}\right)}{(1 + 1/\tilde{C}_{G})[1 + x_{1}\tilde{K}_{d,n1}\Gamma_{1} + (1 - x_{1})\tilde{K}_{d,n2}\Gamma_{2}]},$$
(S25)

where we use $\Gamma_{\alpha} = (1 + \tilde{C}_{G}\tilde{K}_{c,n\alpha})/(1 + \tilde{C}_{G})$, $\tilde{A}_{n} = A_{n}/(\tau_{n}k_{u,n}^{b})$, $\tilde{C}_{G} = C_{G}K_{u,n}$, $\tilde{K}_{d,nq} = K_{d,nq}C$, $\tilde{k}_{c,nq}^{f} = k_{c,nq}^{f}/k_{u,n}^{f}$, $\tilde{K}_{c,nq} = K_{c,nq}/K_{u,n}$ with q = 1, 2. For $x_{1} = 1$, \tilde{A}_{n} reduces to the activity for the single odorant case (Eq. 20 in Ref. [13]).

In Fig. S1, we show \tilde{A}_n as a function of \tilde{C}_G and x_1 , which features a rich landscape depending on the odorant binding constant ratio $(K_{d,n1}/K_{d,n2})$ and relative G-protein binding ratio for odorants of type 1 $(K_{c,n1}/K_{u,n})$. Here, we use $\tilde{k}_{c,n1}^f = \tilde{k}_{c,n2}^f = 100$, $\tilde{K}_{c,n2} = 1$, and $\tilde{K}_{d,n1} = 0.03$, following the parameters considered previously [13]. This means that we keep the agonist condition for odorants of type 2 $(\tilde{k}_{c,n2}^f > \tilde{K}_{c,n2})$ and we vary $\tilde{K}_{c,n1}$, which changes the agonist condition for odorants of type 1. These conditions are depicted by color codes in Fig. S1, in which starting from orange to red, odorants of type 1 become agonists (orange, blue), antagonists (green), and inverse agonists (red), while odorants of type 2 are always agonistic.

When the odorant binding ratio is $K_{d,n1}/K_{d,n2}=0.5$, as shown in Fig. S1(a), the activity is overall a decreasing function of x_1 . This is because odorants of type 2 bind to OR two times faster than type 1, thus the activity is suppressed by increasing x_1 , which becomes less and inverse agonistic as $\tilde{K}_{c,n1}/K_{u,n}$ increases. In Fig. S1(b), when the odorant binding ratio is unity $(K_{d,n1}/K_{d,n2}=1)$, the x_1 -dependency of activity is determined by the agonist condition of odorants of type 2: For $\tilde{K}_{c,n1}=1$ (orange surface) that is actually the same as $\tilde{K}_{c,n2}=1$, two odorant

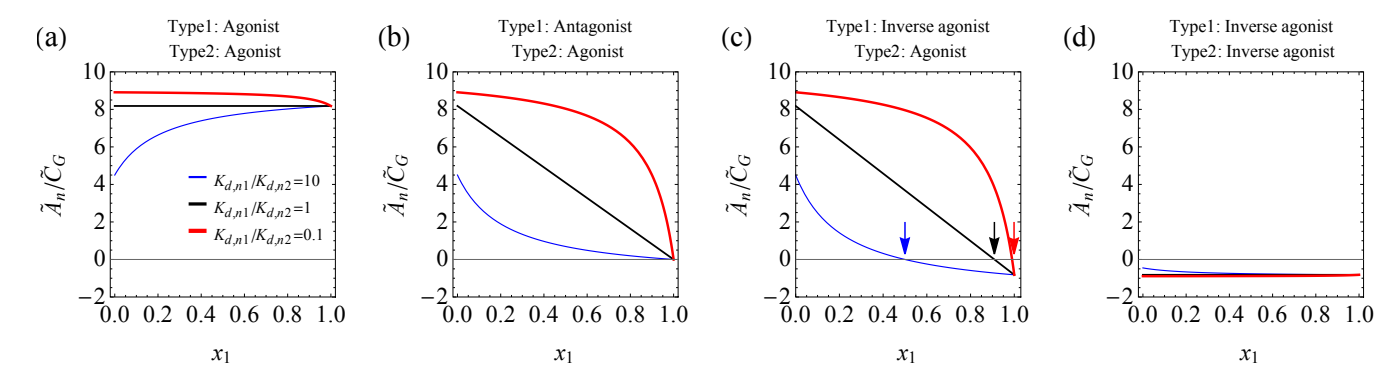


FIG. S2. Odor activity \tilde{A}_n/\tilde{C}_G given in Eq. S27, under the low basal activity condition ($\tilde{C}_G \ll 1$) for (a) both types agonist, (b) type1: antagonist, type2: agonist, type2: agonist, and (d) both types inverse agonist. The arrows in (c) depict the threshold fraction $x_{n1}^{*,\text{low}}$ given in Eq. S29. For an odorant of type α , we use $\tilde{k}_{c,n\alpha}^f = 10$ for the agonist condition, $\tilde{k}_{c,n\alpha}^f = 1$ for the antagonist condition, $\tilde{k}_{c,n\alpha}^f = 0.1$ for the inverse agonist condition, and $\tilde{K}_{d,n1} = 10$.

types are indistinguishable, thus the activity is independent of x_1 and features the s-curve function of G-protein concentration [see orange curves in panels (b-1)-(b-5)]. For $\tilde{K}_{c,n1} > 1$, however, the activity becomes a decreasing function of x_1 because of the fraction of agonistic type 2 decreases. When odorants of type 2 bind two times faster $(K_{d,n1}/K_{d,n2}=10)$, as shown in Fig. S1(c), the activity shows intriguing x_1 -dependent behavior [see panels (c-1)-(c-5)], which can be an increasing function of x_1 under the agonist condition for odorant type 1, otherwise it is a decreasing function of x_1 .

The various behavior of odorant activity arises from the competition between two odorant types with different agonist conditions. Up to $\tilde{K}_{c,n1} = 100$, we find that the activity is positive for all x_1 and C_G . For $\tilde{K}_{c,n1}/K_{u,n} = 1000$ (red), the activity is positive only in a certain limited range of x_1 and C_G [see the crossover of the red lines in Figs. S1(b-1)-(d-5)]. This can be further generalized as the odor activity of a binary mixture is limited by the threshold fraction x_{n1}^* :

$$x_{n1}^*(C_G) = \frac{1}{1 - \frac{\tilde{K}_{d,n1}(\tilde{k}_{c,n1}^f - \Gamma_1)}{\tilde{K}_{d,n2}(\tilde{k}_{c,n2}^f - \Gamma_2)}},$$
(S26)

above which the olfactory signal subtracted by the basal activity, Eq. 12, becomes negative (inverse agonistic), provided that type 2 is agonistic (vice versa, x_{n1}^* is the threshold to be agonistic when type 2 is inverse agonistic).

This agonistic competition in the mixture is well reflected in Figs. S1(b-1)–(c-5), which are cross-sections of $A_n(x_1, \tilde{C}_G)$ in Fig. S1(b) cut for various fixed values of x_1 . The typical s-curve feature of $A_n(C_G)$ for single-type agonistic odorants [Fig. S1(b-1)] changes dramatically when mixed with other odorants of different types with various agonist conditions [Figs. S1(b-2)–(b-4)]. Depending on \tilde{C}_G and the mixing fraction x_1 , the activity can be monotonically agonistic, nonmonotonically agonistic, and even nonmonotonically inverse agonistic. Interestingly, when a small fraction of inverse agonistic odorants is mixed [the red curve in panel (b-2)]. As \tilde{C}_G increases from zero, the activity is maximized and becomes negative as \tilde{C}_G increases further, showing the role of G-protein concentration dramatically controlling the olfactory sensing. This behavior is not found for the single odorant case [panels (b-1) and (b-5)], which is the unique feature arising from a mixture. Another interesting result is found when mixing antagonistic odorants with agonistic odorants [the green curves in panels (b-3) and (b-4)], where the activity is also maximized at an optimal \tilde{C}_G and the mixture becomes agonistic as \tilde{C}_G increases further.

In addition, to explicitly show the effects of the threshold condition x_{n1}^* in Eq. S26 on the activity, we show $A_n(x_1, \tilde{C}_G)$ in Fig. S1(c) cut for various fixed values of \tilde{C}_G in Figs. S1(c-1)–(c-5). As \tilde{C}_G increases, the crossover of the activity is clearly seen in the red curves for the inverse-agonistic odorants of type 1, of which the crossover point is quantified by Eq. S26.

The obtained theoretical result may provide insight into a quantitative analysis of the competitive effect of an odorant mixture.

E. Connection to basal activity

We now consider two limiting cases of the activity, focusing on a connection to the basal activity.

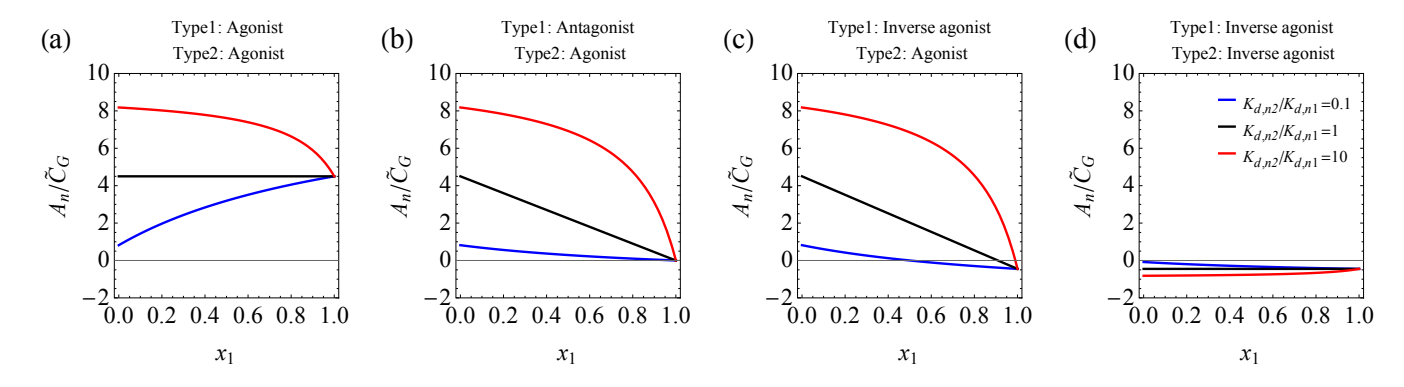


FIG. S3. Odor activity \tilde{A}_n/\tilde{C}_G under low basal activity ($\tilde{C}_G \ll 1$), for (a) both types agonist, (b) type1: antagonist, type2: agonist, (c) type1: inverse agonist, type2: agonist, and (d) both types inverse agonist. For an odorant of type α , we use $\tilde{k}_{c,n\alpha}^f = 10$ for the agonist condition, $\tilde{k}_{c,n\alpha}^f = 0.1$ for the inverse agonist condition, and $\tilde{K}_{d,n1} = 1$.

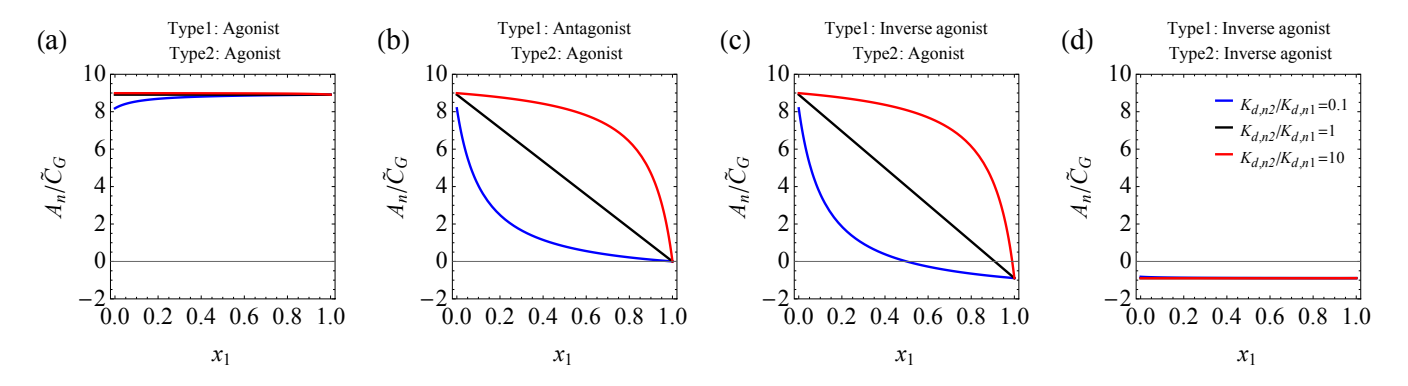


FIG. S4. Odor activity \tilde{A}_n/\tilde{C}_G under low basal activity ($\tilde{C}_G \ll 1$) for (a) both types agonist, (b) type1: antagonist, type2: agonist, (c) type1: inverse agonist, type2: agonist, and (d) both types inverse agonist. For an odorant of type α , we use $\tilde{k}_{c,n\alpha}^f = 10$ for the agonist condition, $\tilde{k}_{c,n\alpha}^f = 1$ for the antagonist condition, $\tilde{k}_{c,n\alpha}^f = 0.1$ for the inverse agonist condition, and $\tilde{K}_{d,n1} = 100$.

First, we focus on the low basal activity condition, under which the binding (or association) constant $(K_{u,n})$ for G-proteins (of constant concentration) to bind to an odorant-unbound OR (u \to G process in Fig. 2) is small, i.e., $\tilde{C}_G \ll 1$. We then find a leading order expression of the activity,

$$\tilde{A}_{n} = \tilde{C}_{G} \frac{x_{1} \tilde{K}_{d,n1} \left(\tilde{k}_{c,n1}^{f} - 1\right) + (1 - x_{1}) \tilde{K}_{d,n2} \left(\tilde{k}_{c,n2}^{f} - 1\right)}{1 + x_{1} \tilde{K}_{d,n1} + (1 - x_{1}) \tilde{K}_{d,n2}}.$$
(S27)

Note that a key quantity that determines the activity is $\tilde{k}_{c,n\alpha}^f$, which is the binding rate of G-proteins to bind to an odorant-bound OR relative to $k_{u,n}^f$. One thus finds that the agonist condition for single-type odorants is $\tilde{k}_{c,n\alpha}^f > 1$. However, for a binary mixture of odorants, we find a criterion for the mixture to be agonist,

$$\frac{K_{d,n1}(\tilde{k}_{c,n1}^f - 1)}{K_{d,n2}(\tilde{k}_{c,n2}^f - 1)} > \frac{x_1 - 1}{x_1}.$$
(S28)

The right-hand side of the above equation is always negative or zero, therefore the inequality holds always when the sign of $\tilde{k}_{c,n1}^f - 1$ and $\tilde{k}_{c,n2}^f - 1$ is the same., i.e., when both types are agonistic or inversely agonistic. This means that for all x_1 , $A_n > 0$ when both types are agonists and $A_n < 0$ when both types are inverse agonists. Interestingly, a crossover of $A_n(x_1)$ can occur when one type is an agonist and the other is an inverse agonist, which controls the activity by x_1 with the threshold condition,

$$x_{n1}^{*,\text{low}} = \frac{1}{1 - \frac{K_{d,n1}(\tilde{k}_{c,n1}^f - 1)}{K_{d,n2}(\tilde{k}_{c,n2}^f - 1)}},$$
(S29)

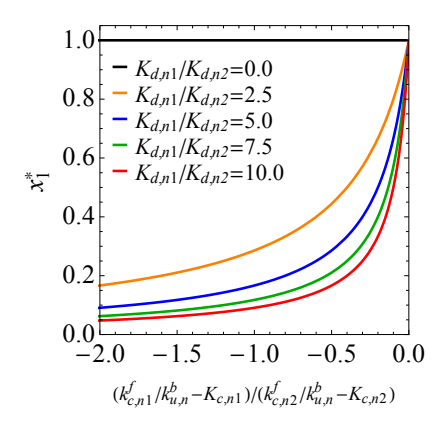


FIG. S5. Threshold odorant fraction $x_{n1}^{*,\text{high}}$ in Eq. S32 as a function of $(k_{c,n1}^f/k_{u,n}^b - K_{c,n1})/(k_{c,n2}^f/k_{u,n}^b - K_{c,n2})$ for different $K_{d,n1}/K_{d,n2}$.

determining of the sign of activity.

Figure S2 shows the activity $\tilde{A}_n(x_1)/\tilde{C}_G$ for different odorant binding rate ratios $K_{d,n2}/K_{d,n1}$ and different agonist conditions. When both odorant types are agonistic, as shown in Fig. S2(a), the mixture is also agonistic and the sign of A_n is always positive for all x_1 . Depending on the odorant binding ratio $K_{d,n2}/K_{d,n1}$, the activity can be a decreasing or increasing function of x_1 , which eventually converges to the value at $K_{d,n2}/K_{d,n1}=1$ as x_1 increases up to unity (the single component limit). This tendency of activity is also found in Fig. S2(b) when odorants of type 1 are antagonistic and type 2 are agonistic, which decreases to zero as x_1 increases. Note that for $K_{d,n2}/K_{d,n1}=1$, the activity becomes a linear function of x_1 . When odorants of type 1 are inverse agonistic and type 2 are agonistic, as shown in Fig. S2(c), we find the crossover of activity as x_1 increases. The threshold fraction $x_{n1}^{*,low}$ given in Eq. S29 is depicted by the arrows in Fig. S2(c). When both odorant types are inverse agonistic, as shown in Fig. S2(d), the mixture is also inverse agonistic and the sign of A_n is always negative for all x_1 . We also show $\tilde{A}_n(x_1)/\tilde{C}_G$ in Figs. S3 and S4 for $\tilde{K}_{d,n1}=1$ and $\tilde{K}_{d,n1}=100$ respectively, of which the overall tendency is similar to Fig. S2.

Figures S3 and S4 show the activity with the same parameters except for $\tilde{K}_{d,n1} = 1$ and $\tilde{K}_{d,n1} = 100$, respectively, of which the overall tendency is similar.

Now suppose that the G-protein-to-OR binding constant $K_{u,n}$ is still small but the concentration of G-protein is exceedingly high, yielding $\tilde{C}_G \gg 1$. This condition can also apply to a case of high basal activity condition when $K_{u,n} \gg 1$, under which the signal downstream can be strong even without odorant-binding events. In the limit of $\tilde{C}_G \to \infty$, we find

$$\tilde{A}_{n} = \frac{x_{1}\tilde{K}_{d,n1}\left(\tilde{k}_{c,n1}^{f} - \tilde{K}_{c,n1}\right) + (1 - x_{1})\tilde{K}_{d,n2}\left(\tilde{k}_{c,n2}^{f} - \tilde{K}_{c,n2}\right)}{1 + x_{1}\tilde{K}_{d,n1}\tilde{K}_{c,n1} + (1 - x_{1})\tilde{K}_{d,n2}\tilde{K}_{c,n2}},$$
(S30)

which yields the agonist criterion,

$$\frac{K_{d,n1}(\tilde{k}_{c,n1}^f - \tilde{K}_{c,n1})}{K_{d,n2}(\tilde{k}_{c,n2}^f - \tilde{K}_{c,n2})} > \frac{x_1 - 1}{x_1}.$$
(S31)

Note that for $x_1 = 1$, one finds $k_{c,n1}^b/k_{u,n}^b > 1$, which is Eq. 22 in Ref. [13], the agonist criterion for the single odorant case. The x_1 -dependency of A_n under this high basal activity condition is well represented in Fig. S1(c-5), in which the crossover occurs at the threshold fraction. The latter is

$$x_{n1}^{*,\text{high}} = \frac{1}{1 - \frac{K_{d,n1}(\tilde{k}_{c,n1}^f - \tilde{K}_{c,n1})}{K_{d,n2}(\tilde{k}_{c,n2}^f - \tilde{K}_{c,n2})}},$$
(S32)

shown in Fig. S5 as a function of $(k_{c,n1}^f/k_{u,n}^b-K_{c,n1})/(k_{c,n2}^f/k_{u,n}^b-K_{c,n2})$, which is positive for negative x-axis values only, meaning a mixture of agonist and inverse agonist.

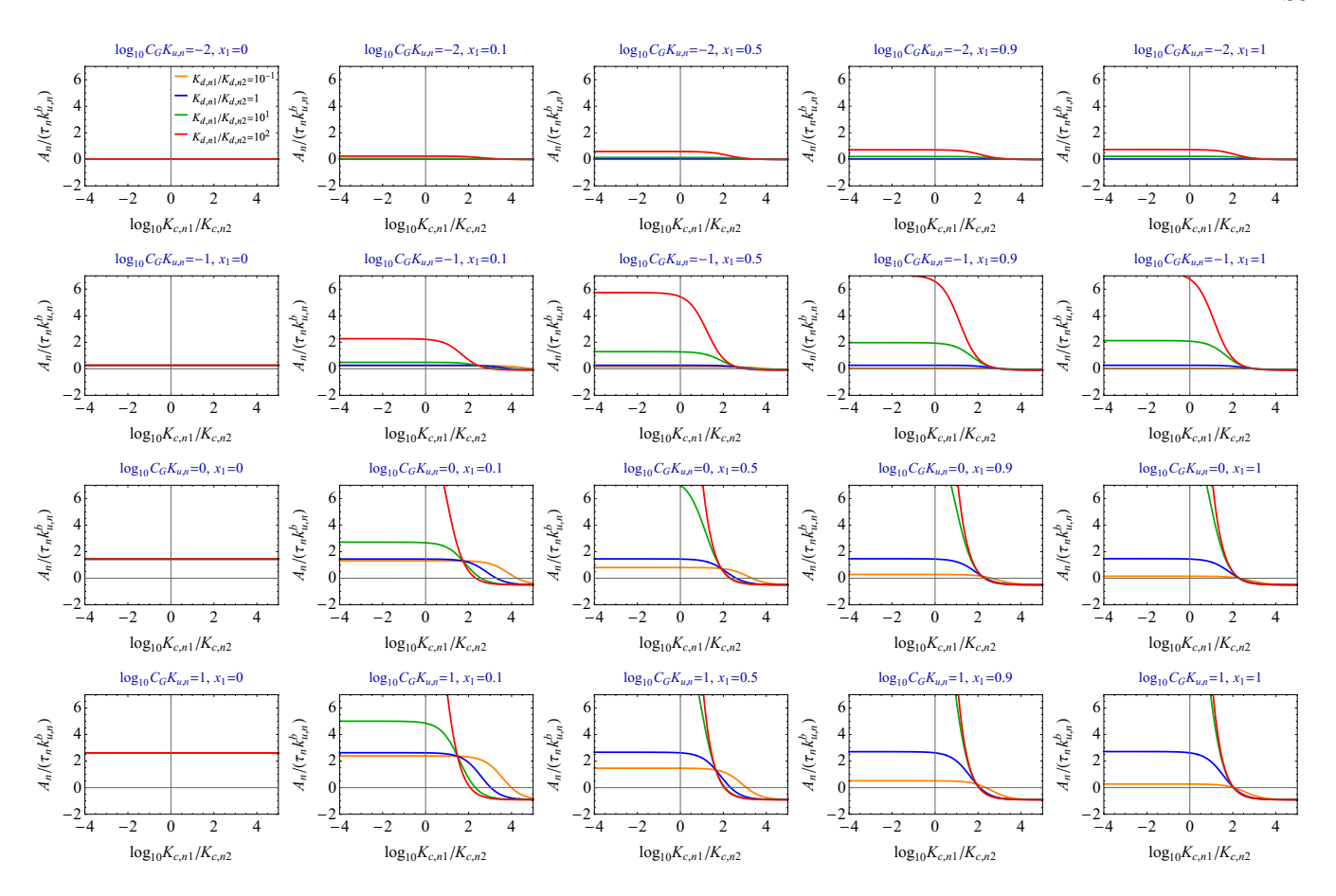


FIG. S6. Odor activity \tilde{A}_n in Eq. S25 as a function of $K_{c,n1}/K_{c,n2}$ at different values of $C_GK_{u,n}$, x_1 and $K_{d,n1}/K_{d,n2}$. We use $\tilde{k}_{c,n1}^f = \tilde{k}_{c,n2}^f = 100$, $\tilde{K}_{c,n2} = 1$, and $\tilde{K}_{d,n2} = 0.03$, following the parameters considered previously [13].

F. Net odor activity depending on $K_{d,nq}$ and $K_{c,nq}$

Here, we present the odor activity A_n given in Eq. S25, now as a function of association constants, $K_{c,n1}/K_{c,n2}$ and $K_{d,n1}/K_{d,n2}$.

Figure S6 depicts the net odor activity $A_n(K_{c,n1}/K_{c,n2})$, which provides an overall profile of activity depending on the G-protein association constants. We also depict the net odor activity $A_n(K_{d,n1}/K_{d,n2})$ in Fig. S7, which shows an overall profile of activity depending on the odorant association constants.

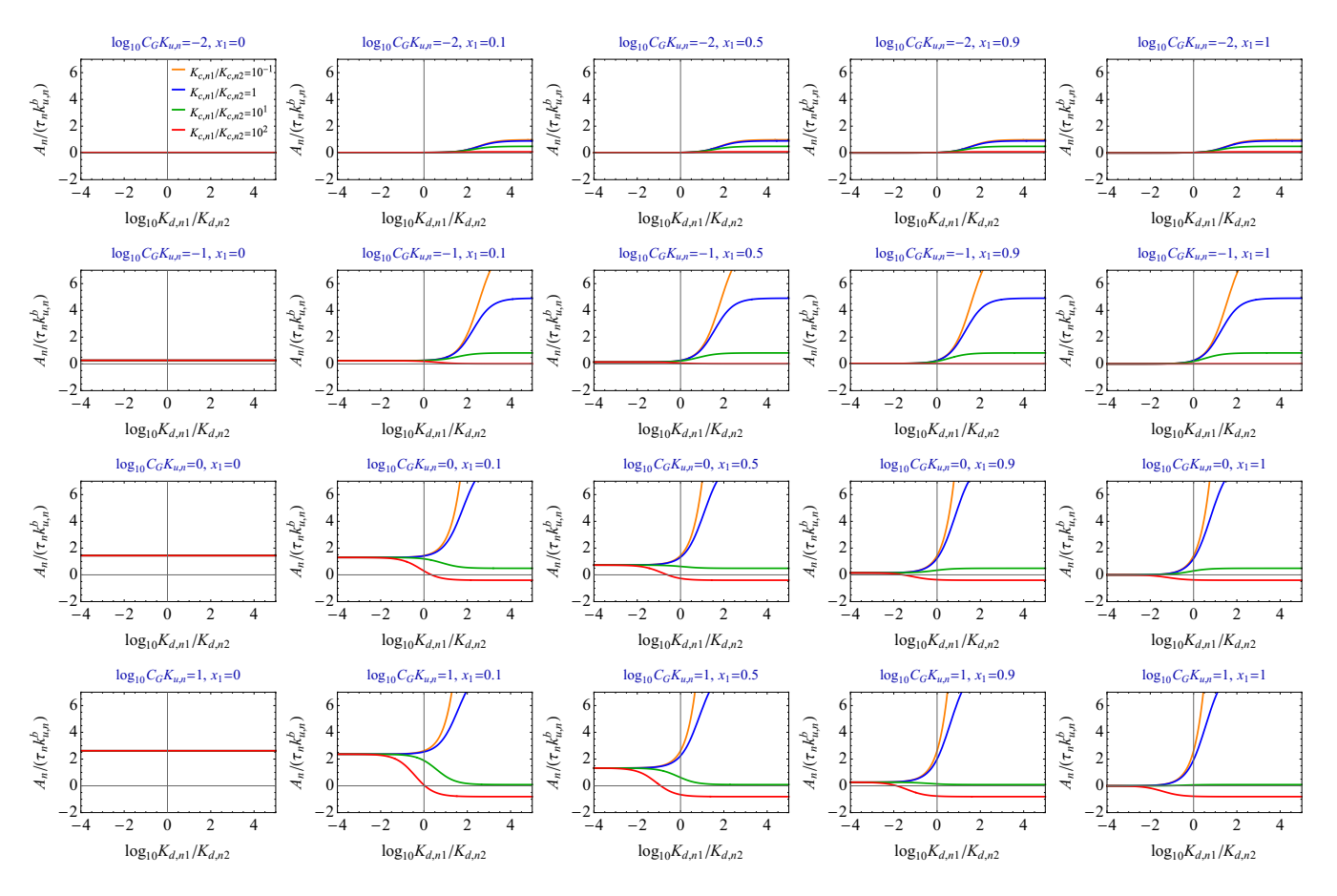


FIG. S7. Odor activity \tilde{A}_n in Eq. S25 as a function of $K_{d,n1}/K_{d,n2}$ at different values of $C_GK_{u,n}$, x_1 and $K_{c,n1}/K_{c,n2}$. We use $\tilde{k}_{c,n1}^f = \tilde{k}_{c,n2}^f = 100$, $\tilde{K}_{c,n2} = 1$, and $\tilde{K}_{d,n2} = 0.03$, following the parameters considered previously [13].